BIOCHEMISTRY
including biophysical chemistry & molecular biology
Article

Biochemistry **2009,** *48,* 11381–11389 11381
DOI: 10.1021/bi901589w

Structural, Thermodynamic, and Kinetic Effects of a Phosphomimetic Mutation in Dynein Light Chain LC8[†]

Gregory Benison, Marcus Chiodo, P. Andrew Karplus,* and Elisar Barbar*

Department of Biochemistry and Biophysics, Oregon State University, Corvallis, Oregon 97331

Received September 10, 2009; Revised Manuscript Received October 27, 2009

ABSTRACT: Dynein light chain LC8 is a small, dimeric, very highly conserved globular protein first identified as an integral part of the dynein and myosin molecular motors but now recognized as a dimerization hub with wider significance. Phosphorylation at Ser88 is thought to be involved in regulating LC8 in the apoptotic pathway. The phosphomimetic Ser88Glu mutation weakens dimerization of LC8 and thus its overall ligand-binding affinity, because only the dimer binds ligands. The 1.9 Å resolution crystal structure of dimeric $LC8_{S88E}$ bound to a fragment of the ligand Swallow (Swa) presented here shows that the tertiary structure is identical to that of wild-type LC8/Swa, with Glu88 well accommodated sterically at the dimer interface. NMR longitudinal magnetization exchange spectroscopy reveals remarkably slow association kinetics ($k_{on} \sim 1\ s^{-1}\ mM^{-1}$) in the monomer−dimer equilibrium of both wild-type LC8 and $LC8_{S88E}$, possibly due to the strand-swapped architecture of the dimer. The Ser88Glu mutation raises the dimer dissociation constant (K_D) through a combination of a higher k_{off} and lower k_{on}. Using a minimal model of titration linked to dimerization, we dissect the thermodynamics of dimerization of wild-type LC8 and $LC8_{S88E}$ in their various protonation states. When both Glu88 residues are protonated, the $LC8_{S88E}$ dimer is nearly as stable as the wild-type dimer, but deprotonation of one Glu88 residue raises K_D by a factor of 400. We infer that phosphorylation of one subunit of wild-type LC8 raises K_D by at least as much to prevent dimerization of LC8 at physiological concentrations. Some LC8 binding partners may bind tightly enough to promote dimerization even when one subunit is phosphorylated; thus linkage between phosphorylation and dimerization provides a mechanism for differential regulation of binding of LC8 to its diverse partners.

Dynein light chain LC8[1] (called DYNLL1 in mammals (*1*)) was first described as an essential component of the dynein (*2*−*4*) and myosin V (*5*) molecular motors, binding directly to specific sites on the dynein intermediate chain IC74 (*6*, *7*) and the myosin V heavy chain (*8*, *9*). Because LC8 also binds to some putative dynein cargos, it has been described as a cargo adaptor (*10*−*12*); however, a large fraction of LC8 is not associated with any molecular motor (*13*), and some of its ligands, such as neuronal nitric oxide synthase (nNOS) (*14*), are not clearly associated with active transport, leading to the emerging concept that LC8 acts as a dimerization hub, binding to diverse partners with some disordered regions and inducing them to dimerize and to form more ordered structures (*6*, *15*, *16*).

Wild-type LC8 can exist as a folded monomer or a folded dimer, with the dimeric form predominating at neutral pH and the monomeric form predominating at low pH (*17*). The disruption of the dimer at low pH has been attributed to protonation of His55, which is solvent-exposed in the monomer with $pK_a \sim 6.5$ and becomes buried at the dimer interface with $pK_a < 4.5$ (*18*). The tertiary structure remains similar in the pH-induced monomer, the apo dimer, and ligand-bound complexes (*19*−*22*). The dimer interface consists of a central β-sheet composed of four strands from one subunit and one strand crossed over from the other subunit (Figure 1). All known ligands bind in a cleft at the dimer interface by appending as a sixth β-strand to the central β-sheet. Both subunits of the dimer contribute to the ligand-binding site, and thus monomeric LC8 fails to bind ligands (*18*, *23*).

Phosphorylation at Ser88 can regulate LC8 *in vivo*. This was first described in the apoptotic pathway, where phosphorylation disrupts binding to BimL, which in turn inhibits apoptosis (*24*−*26*). Initially Pak1, which binds directly to LC8 (*27*), was implicated as the kinase responsible for phosphorylation (*25*); however, this has been questioned (*27*). Despite uncertainty about the kinase involved, the occurrence of LC8 phosphorylation *in vivo* is clear, and its regulatory role is potentially of much broader importance because LC8 is now recognized as a hub protein and general promoter of dimerization involved in numerous pathways (*16*).

Though phosphorylation at Ser88 disrupts ligand binding, Ser88 is not in direct contact with the ligand in any known structure (*21*, *28*), suggesting that phosphorylation does not act by directly occluding the binding site (*23*). Phosphorylation can act primarily by altering quaternary structure, as observed in glycogen phosphorylase (*29*), STAT3 (*30*), and the Kv channel (*31*). In LC8, Ser88 is at the dimer interface, and *in vitro* studies show that the phosphomimetic mutant $LC8_{S88E}$ dimerizes much more weakly than wild-type LC8 (*23*, *26*). The stable LC8 monomer is thus of physiological importance

[†]This work was supported by NSF Grant MCB-0818896 to E.B. and an American Heart Association Fellowship (Award 0720019Z) to G.B. M.C. was supported by an NSF REU award. The OSU Environmental Health Sciences Center is supported by NIH Award NIEHS P30 ES00210.

*Corresponding authors. Phone: (541) 737-4143. Fax: (541) 737-0481. E-mail: barbare@science.oregonstate.edu.

[1]Abbreviations: LC8, 10 kDa dynein light chain; Swa, peptide consisting of residues 281−297 of Swallow; $LC8_{S88E}$, LC8 Ser88Glu mutant.

Published on Web 10/28/2009

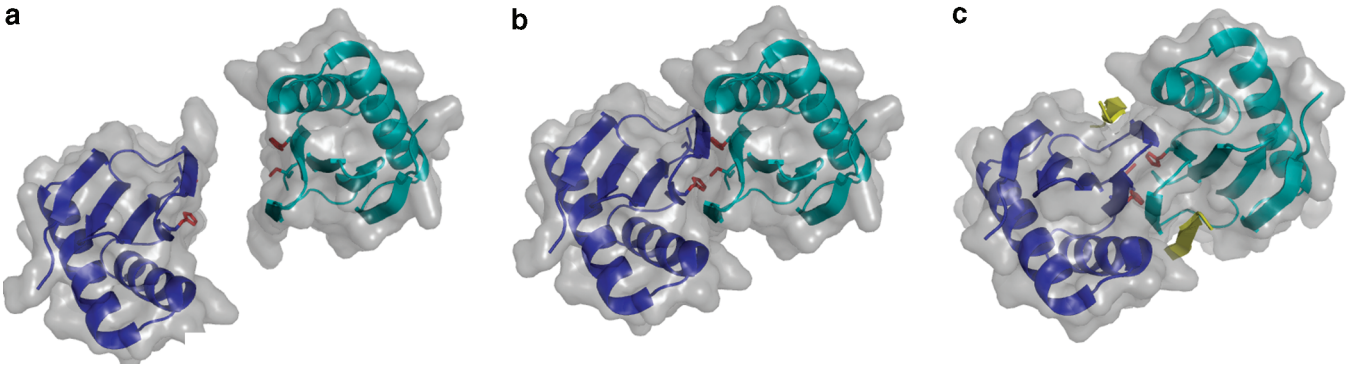

FIGURE 1: Overview of the LC8 structure. (a) In the monomer, His55 and Ser88 (red) are solvent-exposed. The two identical subunits of LC8 are shown in blue and cyan. (b) In the dimer, His55 and Ser88 are buried. Strand β3 forms part of the central β-sheet of the opposite subunit. (c) Ligands (yellow) bind in a cleft at the dimer interface by appending to the central β-sheet. Figure made with PyMol (*41*) using PDB structures 3BRI and 3E2B.

and not just a curiosity of extreme low-pH conditions. Monomeric LC8 cannot bind ligands; therefore, by increasing the monomeric population at the expense of the dimeric population, the Ser88Glu mutation reduces the overall ligand-binding affinity.

The NMR spectra of monomeric, dimeric, and ligand-bound $LC8_{S88E}$ suggest that they are structurally very close to their wild-type counterparts (*23*). The Ser88Glu mutation therefore introduces a titrable group at the dimer interface, which could disrupt the $LC8_{S88E}$ dimer at neutral pH in the same way that His55 disrupts the wild-type dimer at low pH. To test this model of action, we have performed structural, thermodynamic, and kinetic analyses of $LC8_{S88E}$. The crystal structure at 1.9 Å resolution of dimeric $LC8_{S88E}$/Swa is essentially unchanged from that of the wild-type complex. A quantitative model linking dimerization with the titration of interface residues, fit to thermodynamic data for dimer association/dissociation, reveals the energetics of dimerization for wild-type LC8 when both, one, or neither His55 residue is protonated and similarly for $LC8_{S88E}$ in its various protonation states.

NMR spectra of LC8 and $LC8_{S88E}$, recorded at conditions where the dimer dissociation constant is similar to the total protein concentration, contain two distinct sets of signals, corresponding to monomer and dimer. This slow-exchange behavior allows the use of N_Z-exchange spectroscopy (*34*) to compare dimerization kinetics in LC8 and $LC8_{S88E}$. This method offers the advantage of defining both the association and dissociation rates without perturbing the chemical equilibrium (*32*, *33*) and therefore reveals the impact of the phosphomimetic Ser88Glu mutation on the activation energy for dimer dissociation.

EXPERIMENTAL PROCEDURES

X-ray Crystallography. Wild-type LC8, $LC8_{S88E}$, and Swa were prepared as described previously (*20*, *21*, *23*). Crystals were grown at room temperature in hanging drops made by a 1:1 mixture of the reservoir with a stock solution of 1 mM protein and 2 mM peptide in 20 mM Tris-HCl (pH 8.0). The reservoir solution was 0.2 M calcium acetate, 0.1 M sodium cacodylate, and 15% PEG8000, pH 5.5. The crystals grew as hexagonal rods with long axes greater than 300 μm and diameters up to 80 μm and were flash frozen in liquid nitrogen following transfer to a cryoprotectant consisting of reservoir solution plus 20% (v/v) glycerol.

Diffraction data were collected on beamline 5.0.3 at the Advanced Light Source, Berkeley National Laboratories (λ = 1.0 Å; $\Delta\phi$ = 1°; high-resolution pass, 120 10-s images; low-resolution pass, 100 3-s images). Data sets were processed using the HKL suite of programs (*35*). Crystals of $LC8_{S88E}$/Swa belong to space group $P6_122$ with $a = b$ = 44.19 Å and c = 203.22 Å with one molecule in the asymmetric unit and a solvent content of 50%.

Before refinement, 10% of the reflection data were set aside for cross-validation. The test set comprised the same reflections used in the test set for the 2 Å LC8/Swa refinement (*21*), plus new randomly selected reflections beyond 2 Å resolution. The structure was solved by using the LC8 chain from the previously reported LC8/Swa structure (PDB entry 2p1k (*21*)) as a search model for molecular replacment at 3.5 Å resolution using MOLREP (*36*). Rigid body refinement using REFMAC (*37*) resulted in an initial R_{cryst}/R_{free} of 33%/37%. There was strong electron density present for the bound peptide at the rigid body refinement stage. A model for Swa was built into this density, and LC8 residue 88 was changed to Glu. The structure was iteratively refined using REFMAC and Coot (*38*), including TLS refinement (*39*), to R_{cryst}/R_{free} of 19.0%/25.4%. During refinement, ordered water molecules were added or removed by the criterion of having reasonable hydrogen-bonding partners and a peak in the $2F_o - F_c$ electron density map of at least 1σ. Water molecules were numbered on the basis of final peak electron density from 1 (the strongest) to 79 (the weakest).

Per-atom contributions to solvent-accessible surface area were calculated using VOLBL (*40*). Structure diagrams were produced with PyMol (*41*).

The coordinates of the $LC8_{S88E}$/Swa complex have been deposited in the RCSB Protein Data Bank with accession code 3BRL.

NMR Spectroscopy. NMR samples of ^{15}N-labeled wild-type LC8 and ^{15}N-labeled $LC8_{S88E}$ were purified as described previously (*21*, *23*). Samples contained 0.5−1.0 mM protein, 50 mM sodium citrate, 50 mM sodium chloride, 50 mM sodium phosphate, 3% glycerol, and 10% ^2H_2O. pH was in the range 3.0−7.0 and verified to within ±0.1 using an internal maleic acid standard. All NMR experiments were recorded on a Bruker DRX 600 spectrometer at 30 °C. Monomer−dimer exchange rates were measured using N_Z-exchange spectroscopy (*34*). In these experiments, magnetization is first frequency-labeled with the amide nitrogen chemical shift and then after a mixing period is transferred to the amide proton and detected. This leads to four distinct peaks for residues having sufficiently distinct monomer and dimer chemical shifts in both the proton and nitrogen

dimensions: a monomer−monomer autopeak; a dimer−dimer autopeak; and two cross-peaks (monomer−dimer and dimer−monomer) arising from magnetization which has changed environments due to chemical exchange during the mixing period. From the intensities of these four peaks as a function of mixing time, the forward and backward exchange rates can be determined. N_Z-exchange spectra were collected in an interleaved fashion, where the mixing time was incremented before the t_1 delay. For wild-type LC8, mixing times were 150, 300, and 450 ms. For $LC8_{S88E}$, mixing times were 35, 70, 105, 140, 175, and 210 ms.

Peak intensities were determined by fitting signals to two-dimensional Lorenzian lineshapes using in-house software. In fitting the cross-peaks of N_Z-exchange experiments, we constrained the chemical shifts to match the more easily measured autopeaks while allowing the intensity to vary freely. This gives reasonable estimates for the intensities of even very weak cross-peaks, because their position is fixed by the much more intense autopeaks (*33*). Uncertainties in peak intensities were estimated using Monte Carlo sampling. Using the best-fit model as a starting point, model parameters (intensity, line width, peak position) were varied randomly to generate a set of plausible models, accepting only those meeting a χ^2 criterion of $p > 0.05$. Error estimates for the parameters (e.g., peak intensity) were taken as the standard deviations of the parameters within this model set. K_D values were calculated from the intensities of peaks corresponding to monomeric and dimeric populations in $^1H-^{13}C$ CT-HSQC spectra (for wild-type LC8 (*18*)) or $^1H-^{15}N$ HSQC spectra (for $LC8_{S88E}$) with a 3 s recycle time. Error estimates for K_D were calculated by standard error propagation rules from errors in the peak intensities.

Peak volume as a function of time ($\dot{I}$) was modeled by the Bloch equations for two-site exchange between a monomeric environment (M) and a dimeric environment (D):

$$[\dot{I}_M] = -k_+[I_M] + k_-[I_D] - R_M[I_M] \quad (1)$$

$$[\dot{I}_D] = k_+[I_M] - k_-[I_D] - R_D[I_D] \quad (2)$$

where R_M and R_D are the T_1 relaxation rates for monomer and dimer, respectively. The forward and backward magnetization exchange rates k_+ and k_- are equivalent to the chemical exchange rates for a unimolecular reaction such as protein unfolding (*34*). For this bimolecular reaction, they are determined by the relations $k_+ = k_{on}M$ and $k_- = k_{off}$, where k_{on} and k_{off} are the rate constants of the $LC8_{S88E}$ dimerization equilibrium:

$$2M \underset{k_{off}}{\overset{k_{on}}{\rightleftharpoons}} D \quad (3)$$

The monomer concentration M is a constant and can be calculated from the (known) total protein concentration and the rate constants k_{on} and k_{off}; therefore, k_{on} and k_{off} are sufficient to determine k_+ and k_- .

An error function was calculated as the sum of squared residuals between measured and predicted peak volumes. For each residue, the fitting procedure included both cross-peaks and both autopeaks. When too weak to measure, the cross-peak intensity was set to an upper bound of 1 (expressed as a signal-to-noise ratio) for fitting purposes, leading in turn to an upper bound on the kinetic constants. The kinetic parameters k_{on} and k_{off}, when fit on a per-residue basis, clustered within a distribution of ~±50%, suggesting that modeling the data as the result of a single exchange process affecting the entire protein was justified. Therefore, we performed a global fit in which monomer and dimer initial peak intensities were independent parameters for each residue, but rate constants were constrained to be equal for all residues. The predicted volume was thus a function of the four independent parameters, k_{on}, k_{off}, R_M, and R_D, in addition to two independent parameters (I_M^o and I_D^o) for each residue included in the fit.

The best-fit parameters were determined by a gradient-descent search, with error estimates on parameters derived from the gradient at the minimum. The minimization and the solution of the differential equations involved in fitting were both performed using the numerical package R (www.r-project.org).

Minimal Model. To explain the pH dependence of k_{on}, k_{off}, and K_D, we developed a minimal model based on coupled equilibria of protein dimerization and titrating residues at the dimer interface. Our model is an adaptation of one that has been used to explain the pH dependence of folding kinetics in an SH3 domain (*42*).

Our model for wild-type LC8 includes His55 as the sole titrable residue at the dimer interface. In such a system, the dimer can form by three distinct pathways: association of two unprotonated monomers, association of one protonated and one unprotonated monomer, or association of two protonated monomers (Scheme 1). The acid dissociation constant in the monomeric state (pK_a^M) and the first and second acid dissociation constants in the dimeric state (pK_a^{D1} and pK_a^{D2}) are not generally equal, because the titrating group is in a different environment. Because of thermodynamic cycles linking protonation to dimerization, of the six parameters in this model (three acid dissociation constants and three dimer dissociation constants) only four can be varied independently.

We extended the model to $LC8_{S88E}$ by incorporating titration of Glu88, leading to additional parameters and thermodynamic cycles. In general, the overall free energy of association as a function of pH is given by

$$\Delta\Delta G^\circ_{M\to D} = RT\sum_i \ln\frac{([H^+]+K^M_{a,i})^2}{[H^+]^2 + 2[H^+]K^{D1}_{a,i} + K^{D1}_{a,i}K^{D2}_{a,i}} \quad (4)$$

where the sum extends over all titrating residues.

Kinetic predictions can be obtained by considering pK_a values in the transition state as well as in the monomeric and dimeric states. For a protein dimerization reaction, the transition state is itself dimeric and resembles the bound state (*43*, *44*). Overall kinetic behavior in the presence of titrating groups can be described in terms of a pH-dependent free energy for the initial state, the final state, and a transition state ensemble (*42*):

$$\Delta\Delta G^\circ_{M\to ‡} = RT\sum_i \ln\frac{([H^+]+K^M_{a,i})^2}{[H^+]^2 + 2[H^+]K^{‡1}_{a,i} + K^{‡1}_{a,i}K^{‡2}_{a,i}} \quad (5)$$

$$\Delta\Delta G^\circ_{D\to ‡} = RT\sum_i \ln\frac{[H^+]^2 + 2[H^+]K^{D1}_{a,i} + K^{D1}_{a,i}K^{D2}_{a,i}}{[H^+]^2 + 2[H^+]K^{‡1}_{a,i} + K^{‡1}_{a,i}K^{‡2}_{a,i}} \quad (6)$$

where M, D, and ‡ are the monomeric, dimeric, and transition states, respectively. The sum contains one term for each titrating group at the interface.

Scheme 1: Model of Titration-Linked Dimerization[a]

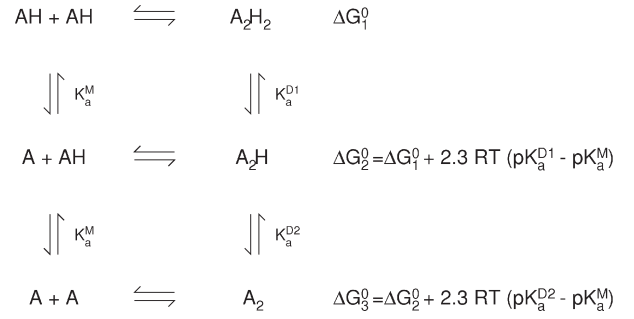

[a]Abbreviations: A, unprotonated monomer; AH, protonated monomer; A_2, unprotonated dimer; A_2H, singly protonated dimer; A_2H_2, doubly protonated dimer.

From the free energies of the monomeric, dimeric, and transition states, we can calculate dimer dissociation equilibrium and rate constants:

$$RT \ln K_D = \Delta G^\circ_{M \rightarrow D} \quad (7)$$

$$-RT \ln k_{on} = -RT \ln\left(\frac{\kappa k_b T}{h}\right) + \Delta G^\circ_{M \rightarrow \ddagger} \quad (8)$$

$$-RT \ln k_{off} = -RT \ln\left(\frac{\kappa k_b T}{h}\right) + \Delta G^\circ_{D \rightarrow \ddagger} \quad (9)$$

where k_b and h are the Boltzmann and Planck constants, respectively, and κ is a transmission coefficient.

For wild-type LC8, His55 pK_a^M, pK_a^{D1}, and pK_a^{D2} were set initially to the acid dissociation constant of free histidine and then iteratively adjusted to give the best least-squares fit simultaneously to K_D, k_{on}, and k_{off} according to eqs 7, 8, and 9. Experimental K_D values were taken from ref *18*, and k_{on} and k_{off} were taken from this study. For $LC8_{S88E}$, titration of His55 and Glu88 was considered. Though the acid dissociation constants for His55 in $LC8_{S88E}$ may differ from those in wild-type LC8, the amount of available data did not justify fitting the pK_a values for both residues independently. Thus, to model $LC8_{S88E}$, we used the acid dissociation constants of His55 from wild-type LC8 and adjusted the acid dissociation constants of Glu88 iteratively to give the best match to the experimentally measured K_D, k_{on}, and k_{off}.

RESULTS

Crystal Structure of $LC8_{S88E}$. The structure of $LC8_{S88E}$/Swa was solved by rigid body refinement using the LC8 chain from the wild-type LC8/Swa complex (*21*) as the initial model and refined at 1.9 Å resolution to R_{cryst} = 19.0% and R_{free} = 25.4% (Table 1). All residues were in the most favored Ramachandran region except for Asn51, which as in all LC8 structures has a positive ϕ angle and is part of a turn which also features a *cis*-peptide bond between Pro52 and Thr53. Electron density clearly shows the conformation of Glu88 (Figure 2a). The structure of $LC8_{S88E}$/Swa is nearly identical to that of wild-type LC8/Swa (C^α rmsd of 0.28 Å), and even at the site of mutation, the backbone and side chain torsion angles are similar (Figure 2b). In wild-type LC8, Ser88′ O has two hydrogen bond donors: Ser88 Oγ and His55 Nε. In S88E, the hydrogen bond from Ser88 Oγ is lost. Instead, the methylene group of Glu88 is in steric contact with Glu88′ O, at a favorable nonbonded distance (*45*). Glu88 adopts a rotamer directing the side chains away from each other, such that the distance between the carboxylates is 7 Å (Figure 2a). The Glu88 side chain is mostly buried in a pocket formed by residues Thr53, His55, and Thr67′, with the carboxylate group only partially exposed (18 $Å^2$ solvent-accessible surface compared with 60−80 $Å^2$ for the most exposed carboxylate groups).

Table 1: Data Collection and Refinement Statistics

resolution	∞−1.90 (2.01−1.90)
reflections (total/unique)	195803/10183
completeness	100.0 (99.8)
R_{meas}[a]	9.6 (72.4)
I/σ	27.9 (3.8)
refinement	
resolution (Å)	∞−1.90 (1.95−1.90)
no. of reflections	9605 (685)
no. of amino acids (LC8)	88
no. of amino acids (ligand)	10
no. of solvent atoms	79
total no. of atoms	880
average B (all atoms) ($Å^2$)	34
R_{cryst}(%)	19.0 (22.0)
R_{free}(%)	25.4 (27.3)
rmsd bonds (Å)	0.009
rmsd angles (deg)	1.1
ϕ, ψ most favored[b]	96/97

[a]As defined by Diederichs and Karplus, 1997. [b]As defined in Lovell et al., 2003.

Thermodynamics of Dimerization. In HSQC spectra of wild-type LC8 in the pH 4.2−5.3 range, and those of $LC8_{S88E}$ in the pH 4.2−6.7 range, certain residues (primarily those at the dimer interface) have two distinct peaks, corresponding to monomer and dimer. Changing the pH, and thus the monomer/dimer populations, alters the intensities but not the positions of these peaks (i.e., they are in the NMR slow-exchange regime), allowing determination of K_D through ratios of peak intensities (Figure 3). The K_D of wild-type LC8 decreases monotonically with increasing pH with a midpoint at pH 4.5, reaching a limit <1 μM at high pH (*18*). The pH dependence of $LC8_{S88E}$ dimerization is remarkably different (Figure 4; Supporting Information Table 1): K_D decreases with increasing pH until reaching a minimum of K_D = 930 μM at pH 5.5 and then increases again at higher pH. We attribute these opposing trends to perturbation of titrating residues at the dimer interface: in the dimer, the pK_a of His55 is lowered, and that of Glu88 is elevated.

To show that dimerization coupled to titration of residues at the interface can quantitatively account for the different pH dependence of K_D for wild-type LC8 and $LC8_{S88E}$, we developed a minimal model (see Experimental Procedures). We began by constructing a model of wild-type LC8 considering only titration of His55. In fitting K_D vs pH, the freely variable parameters were pK_a^M (the acid dissociation constant in the monomer), pK_a^{D1} and pK_a^{D2} (the acid dissociation constants in the dimer), and either ΔG°_1 or ΔG°_3 (Scheme 1). It was not possible to fit all four parameters simultaneously through global fitting procedures, but by iterative refinement from reasonable starting values, we found a local best fit (Table 2). The model based on the best-fit parameters accurately reproduced experimentally measured K_D over the pH 3−7 range (Figure 4). To test the robustness of the reported parameters, we performed systematic searches around the best-fit values (Figure 5). All good fits had the following

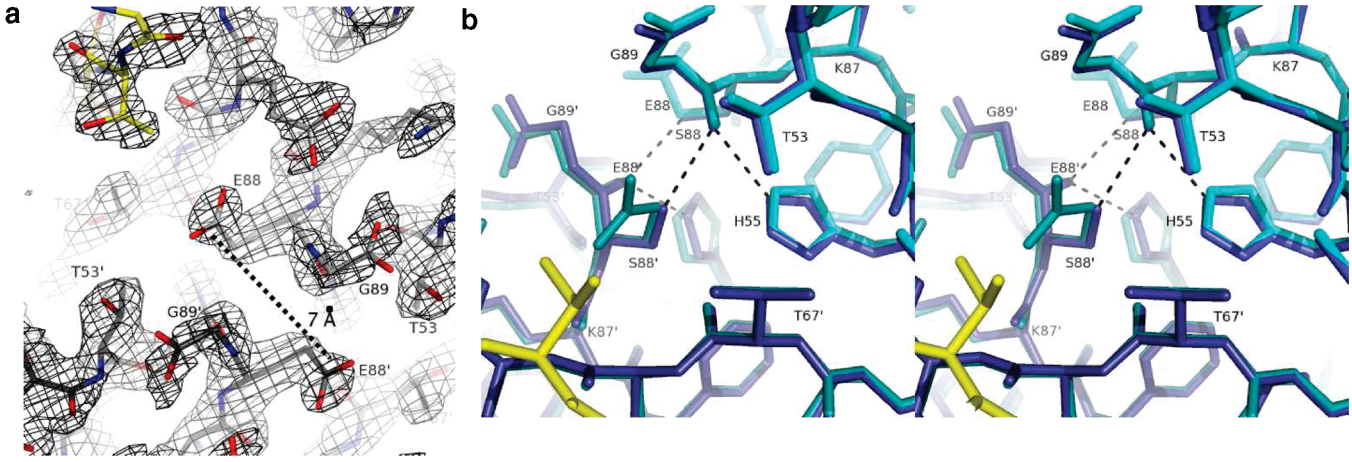

FIGURE 2: Crystal structure of $LC8_{S88E}$ showing the environment of Glu88. (a) Electron density for Glu88 in $LC8_{S88E}$/Swa. View is along the 2-fold symmetry axis with $2F_o - F_c$ density contoured at 1.2σ and showing $LC8_{S88E}$ (cyan) and the peptide (yellow). (b) Stereoview of the environment of residue Ser88 in wild-type LC8/Swa (blue) and of residue Glu88 in $LC8_{S88E}$/Swa (cyan). The peptide is shown in yellow. Chain B is shown in a darker shade than chain A. Figure made with PyMol (*41*) using PDB structures 3BRL ($LC8_{S88E}$/Swa) and 3E2B (LC8/Swa).

properties: pK_a^M in the range 6.0−6.5, as expected for an exposed histidine; pK_a^{D1} and pK_a^{D2} less than 4.5; and $\Delta G°_3$, the free energy of association in the limit of high pH, below 0.3 μM.

The model of $LC8_{S88E}$ considered titration of His55 and Glu88. We retained the best-fit parameters for His55 from the wild-type model and iteratively adjusted the parameters of Glu88. As for wild-type LC8, the model accurately reproduced the experimental measurement of K_D (Figure 4), including the opposite trends for wild-type LC8 vs $LC8_{S88E}$ over the pH 5−7 range. We used a grid search to investigate the robustness of the pK_a values (Figure 5). The best-fit pK_a^M of Glu88 is 4.2, near its unperturbed value in the free amino acid. A good fit required that Glu88 $pK_a^{D1} > 6$ and Glu88 $pK_a^{D2} > 7$, with best-fit values of 6.8 and 7.5. The initial fit was performed when only three of the six K_D measurements for $LC8_{S88E}$ were available (see points marked with an asterisk in Figure 4). The later collected points, despite their not being included in the initial fit, were in good agreement with the model, serving as a cross-validation of the modeling approach and best-fit parameters. When all of the data were included in the fit, the best-fit pK_a values remained unchanged to within 0.1 unit.

Using the relationships in Scheme 1, we calculated separate K_D values for LC8 in its distinct protonation states (Table 3). For wild-type LC8, the most tightly dimerizing form (K_D = 0.06 μM) is that in which neither His55 is protonated, corresponding to the limiting K_D at high pH. The most weakly dimerizing form (K_D = 21000 μM) is that in which both His55 residues are protonated, corresponding to the limiting K_D at low pH. Similarly, for $LC8_{S88E}$, the most tightly dimerizing form (K_D = 0.07 μM) is that in which all titrating residues are neutral, and the most weakly dimerizing form ($K_D = 1.8 \times 10^{10}$ μM) is that in which all titrating residues are charged. Interestingly, these states, unlike those of wild-type LC8, do not predominate at any pH and thus do not correspond to any observable limit. Over the pH range studied (4.0−6.7), the observed macroscopic K_D of $LC8_{S88E}$ reflects a mixture of protonation states and reaches a minimum of 0.9 mM at pH 5.2.

Kinetics of Dimerization. We measured dimer association rate constants (k_{on}) and dimer dissociation rate constants (k_{off}) for wild-type LC8 and $LC8_{S88E}$ using N_Z-exchange NMR spectroscopy (*34*) (Figure 3). For four residues (Asp37, Gly59, Gly63, and Ala82) both cross-peaks and both autopeaks were sufficiently resolved to allow quantitative measurements of exchange rates: for wild-type LC8 between pH 4.2 and pH 5.3, k_{off} = 0.05−0.24 s^{-1} and k_{on} = 1.0−3.0 s^{-1} mM^{-1}; for $LC8_{S88E}$ between pH 5.5 and pH 6.7, k_{off} = 1.9−5.7 s^{-1} and k_{on} = 1.2−3.0 s^{-1} mM^{-1} (Figure 4 and Supporting Information Table 1).

The rate constants for dimerization are pH-dependent, which we explained by extending the model to include acid dissociation constants in the transition state ($pK_a^{‡1}$ and $pK_a^{‡2}$). These were iteratively adjusted to match the kinetic data, resulting in best-fit values intermediate between those in the monomeric and dimeric states. The resulting model accurately reproduced the experimentally measured rate constants for wild-type LC8 and $LC8_{S88E}$ (Figure 4).

DISCUSSION

Phosphorylation of Ser88 regulates LC8 by weakening its dimerization, which in turn diminishes overall affinity for ligands which can bind only to the dimer (*23*, *25*, *26*). Our biophysical studies of $LC8_{S88E}$ as a phosphomimetic mutant probe the origin of this weakened dimerization. NMR spectra first suggested that $LC8_{S88E}$/Swa is structurally very close to its wild-type counterpart (*23*), and this is now confirmed by the crystal structure (Figure 2B). We have measured dimer stability and dimerization kinetics as a function of pH for both wild-type LC8 and $LC8_{S88E}$. Using a minimal model, we dissect the thermodynamics and kinetics of association for wild-type LC8 and $LC8_{S88E}$ in their various protonation states.

Dimer Disruption by Titrating Residues at the Interface. Previously, we showed that titration of His55, uniquely among the histidine residues of LC8, is linked thermodynamically to dimerization (*18*). When His55 is protonated, formation of the dimer would result in the unfavorable burial of a charge at the interface. His55 and His55′ are in close proximity in the dimer, leading to an additional energetic penalty from like-charge repulsion when both are protonated. Glu88, like His55, is buried at the dimer interface near its symmetry mate. To demonstrate that titration of these two residues sufficiently explains the pH dependence of dimerization, we constructed a minimal model incorporating only His55 (for wild-type LC8) or His55 and Glu88 (for $LC8_{S88E}$) that accurately reproduces K_D over a wide pH range (Figure 4A).

From the best-fit model parameters, we calculated the energetics of dimerization in all possible protonation states (Table 3), allowing us to assess the relative importance of burial of a single charge

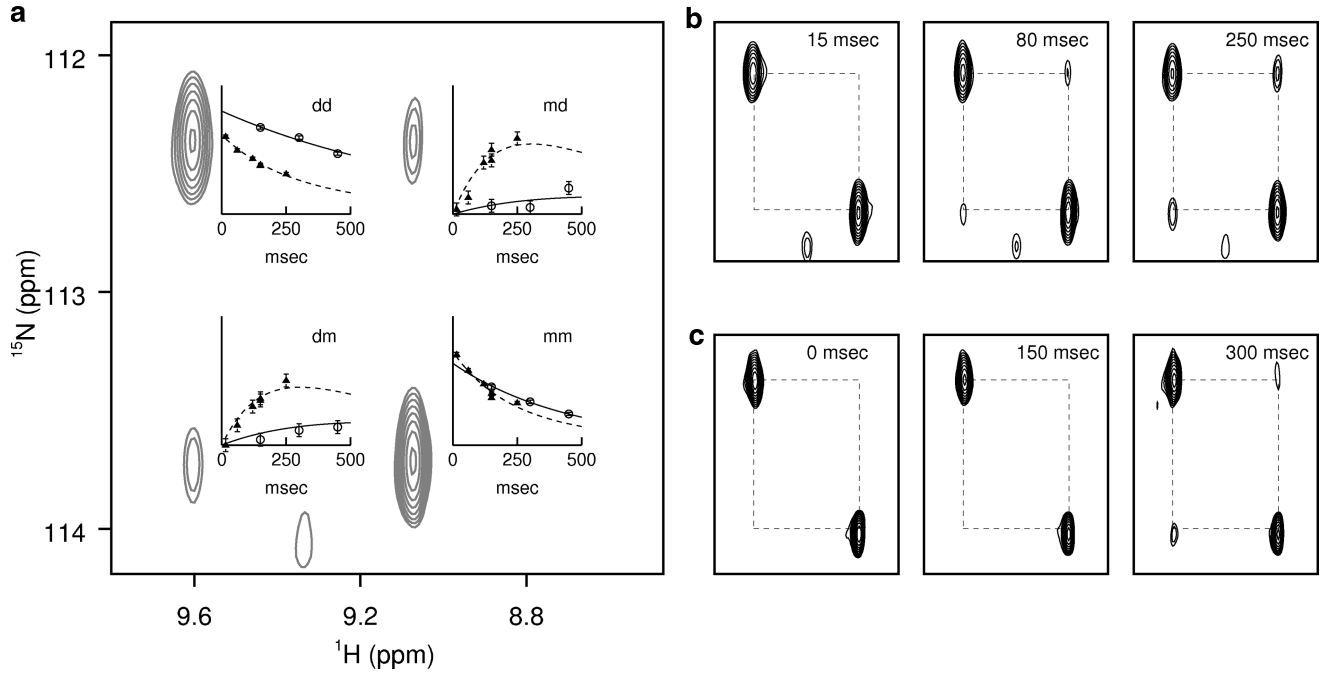

FIGURE 3: Monomer−dimer exchange kinetics measured by NMR. (a) Excerpt around residue 59 from an N_Z-exchange spectrum of $LC8_{S88E}$. The relative peak intensity as a function of mixing time (wild-type, circles; $LC8_{S88E}$, triangles) is plotted beside each of the four component peaks (dd, dimer−dimer autopeak; mm, monomer−monomer autopeak; dm, dimer−monomer cross-peak; md, monomer−dimer cross-peak). The vertical scale of the dd and mm plots is four times that of the md and dm plots. The fits to eq 1 are shown as solid lines (wild-type LC8) or dashed lines ($LC8_{S88E}$). (b) Excerpts of the same region from additional N_Z-exchange spectra at different mixing times, showing the buildup of the cross-peaks. (c) Similarly for wild-type LC8.

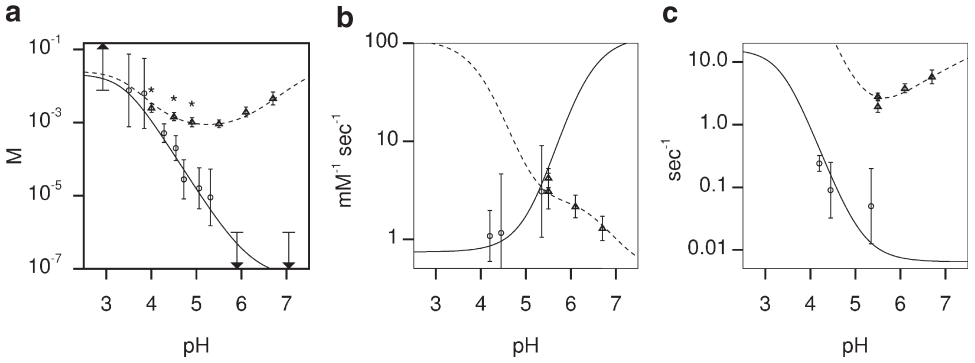

FIGURE 4: pH dependence of kinetic and thermodynamic parameters for LC8 dimerization: (a) K_D, (b) k_{on}, and (c) k_{off}. Experimental data points are shown as circles for wild-type LC8 and as triangles for $LC8_{S88E}$. The best-fit model is shown as solid lines for wild-type LC8 and dashed lines for $LC8_{S88E}$. The experimental data also appear in Supporting Information Table 1. Arrows indicate measurements which are upper or lower bounds. Data points collected after initial model fitting are marked with asterisks (see Results).

vs like-charge repulsion between symmetry mates. For wild-type LC8 in the limit of high pH (conditions where His55 is entirely deprotonated in both the monomer and dimer), the calculated K_D is 0.06 μM, which is consistent with a recently reported experimental upper bound of 0.5 μM at pH 7.4 (*27*). The burial of one charged His55 residue destabilizes the dimer by 3.3 kcal/mol, corresponding to a 250-fold rise in K_D (Table 3). Protonation of the second histidine residue incurs an additional energetic penalty of 4.4 kcal/mol, equivalent to a 1500-fold rise in K_D. We attribute the greater energetic penalty (by 1.1 kcal/mol) of the second deprotonation to like-charge repulsion between His55 and His55′. This is in reasonable agreement with an expected penalty of 1.6 kcal/mol calculated by considering His55 and His55′ as point charges separated by 6 Å (the distance between the imidazole rings in the crystal structure) and estimating an effective dielectric constant of 40 (taken from a variety of mutagenesis and titration studies of charged residues at or near the protein surface (*46*−*48*)).

Table 2: Acid Dissociation Constants in the Monomeric, Dimeric, and Transition States Derived from the Minimal Model of Titration-Linked Dimerization[a]

	His55	Glu88
pK_a^M	6.2	4.2
pK_a^{D1}	3.0	6.8
pK_a^{D2}	3.8	7.5
$pK_a^{\ddagger 1}$	4.9	6.0
$pK_a^{\ddagger 2}$	5.3	7.0

[a]The pK_a values for His55 were obtained by fitting the model to the wild-type data and were fixed to be the same in both the wild-type and $LC8_{S88E}$ models (as described in Experimental Procedures).

For states of $LC8_{S88E}$ in which both Glu88 and Glu88′ are protonated, K_D is only slightly higher than that for the corresponding states of wild-type LC8 (Table 3). Therefore, steric effects and/or loss of intersubunit hydrogen bonds involving

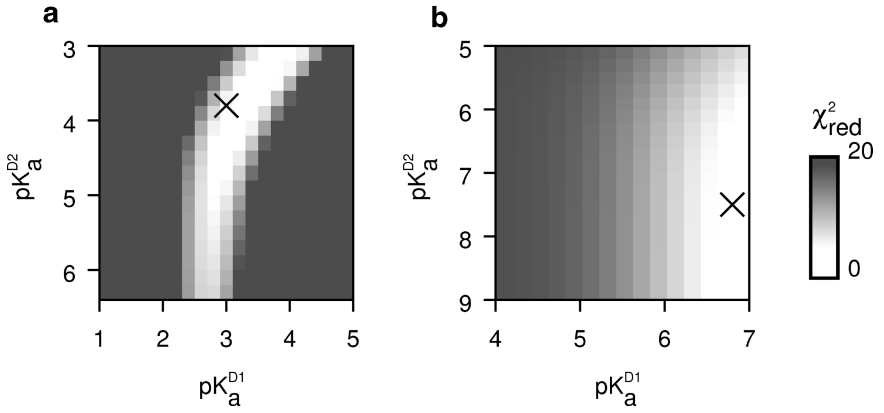

FIGURE 5: Exploration of the robustness of the model parameters near the best fit. (a) Grid search of His55 pK_a^{D1} and pK_a^{D2} in wild-type LC8. (b) Grid search of Glu88 pK_a^{D1} and pK_a^{D2} in LC8$_{S88E}$. The cross symbol marks the location of the best-fit parameters. The goodness of fit, reported as a reduced χ square value, is shown for the surrounding parameter space.

Table 3: Dimer Dissociation Constants (in μM) for Wild-Type LC8 (wt) and LC8$_{S88E}$ in All Possible Distinct Protonation States, Derived from the Titration-Linked Model

		LC8$_{S88E}$		
	wt	Glu$_{88}$/Glu$_{88}$	Glu$_{88}$/Glu$^-_{88}$	Glu$^-_{88}$/Glu$^-_{88}$
His$^+_{55}$/His$^+_{55}$	2.1×10^4	2.5×10^4	1.1×10^5	1.8×10^{10}
His$_{55}$/His$^+_{55}$	14	17	6800	1.2×10^7
His$_{55}$/His$_{55}$	0.060	0.071	28	5.9×10^4

Ser88, which have been proposed as mechanisms for the disruption of the LC8$_{S88E}$ dimer (*23*, *26*), appear to play a minor role. This is consistent with the crystal structure of LC8$_{S88E}$/Swa, which shows Glu88 easily accommodated sterically at the dimer interface, and with the thermodynamics of LC8$_{S88A}$, which also lacks the hydrogen bonds involving Ser88 yet remains strongly dimeric (*49*). It is only when the Glu88 side chain is deprotonated that the Ser88Glu mutation becomes disruptive: the first deprotonation destabilizes the dimer by 3.6 kcal/mol, raising K_D 400-fold. The second deprotonation destabilizes the dimer by 4.5 kcal/mol and raises K_D an additional 2000-fold. We attribute the 0.9 kcal/mol higher penalty to like-charge repulsion between Glu88 and Glu88′, in reasonable agreement with the expected penalty of 1.4 kcal/mol calculated for two point charges separated by 7 Å (the distance between the carboxylates in the crystal structure).

Impact of the Ser88Glu Mutation on Dimerization Kinetics. N_Z-exchange spectroscopy has been used to measure the kinetics of the folding−unfolding transition of an SH3 domain (*34*) and of protein dimerization in type II cadherin (*50*). The method requires that both states are similarly populated and that exchange rates are in the appropriate range of 0.5−10 s^{-1} (*32*, *34*, *51*). These conditions are satisfied for monomer−dimer exchange in wild-type LC8 over the pH 4.2−5.3 range and for LC8$_{S88E}$ over the pH 5.5−6.7 range. Dimer association of both wild-type LC8 and LC8$_{S88E}$ is remarkably slow: the observed k_{on} values of 1.0−2.0 s^{-1} mM^{-1} are at the low end of the range seen for protein−protein interactions, an order of magnitude below typical values and a million times lower than the fastest, diffusion-limited protein−protein association rates (*52*). The slow kinetics may reflect the complexity of the dimerization process for LC8, which is not a simple association of complementary surfaces; rather, a disordered strand in each monomer is incorporated into a β-sheet, requiring formation of several new intersubunit hydrogen bonds (*53*).

We measured the rates for LC8$_{S88E}$ at near-neutral pH (6.7), but for wild-type LC8 measurements are not possible above pH 5.3 because the monomer population is too low to detect by NMR. Using the model, however, we can extrapolate to neutral pH, obtaining $k_{on} = 89$ s^{-1} mM^{-1} for wild-type LC8 and $k_{on} = 1$ s^{-1} mM^{-1} for LC8$_{S88E}$ (Figure 4B). Thus at physiological pH the Ser88Glu mutation not only disrupts the dimer but also greatly slows association and, hence, raises the free energy of the transition state as well as that of the dimeric state (Figure 6).

Dimerization Coupled to Ligand Binding. Dissociation of LC8 to monomers, by decreasing the amount of dimer available to bind ligands, decreases the apparent ligand affinity. The effective ligand-binding constant K'_L, taking into account the ligand-binding sites that become unavailable due to dimer dissociation (see Scheme 2), is

$$K'_L = K_L \frac{\left(1 + \frac{1}{2}\sqrt{\frac{K_D}{D}}\right)K_L + L}{K_L + L} \quad (10)$$

For example, consider a 1:1 mixture at 10 μM of LC8 and the dynein intermediate chain (IC), which binds with an affinity of 3 μM (*53*). K_D of wild-type LC8 at neutral pH is less than 0.1 μM, so dimer dissociation lowers the effective ligand affinity by only 1%. In contrast, K_D for LC8$_{S88E}$ is 7 mM, leading to a 4-fold decrease in effective ligand affinity. Thus dimer dissociation explains the results of GST pulldown experiments in which LC8$_{S88E}$ bound IC with only about half the efficiency of wild-type LC8 (*23*), even if the intrinsic ligand affinity (K_L) is the same for both wild-type LC8 and LC8$_{S88E}$. Similarly, in a fluorescence assay at micromolar concentration a complex of wild-type LC8 and the ligand Bim formed to completion, yet only a small amount of LC8$_{S88E}$/Bim was detected even when LC8$_{S88E}$ was present in 50-fold excess (*26*).

Binding of ligands to the dimer also decreases the apparent dimer dissociation constant K'_D in the presence of ligands (Scheme 2):

$$K'_D = K_D\left(\frac{K_L}{K_L + L}\right)^2 \quad (11)$$

This explains the observation that LC8$_{S88E}$ at 0.2 mM is mostly monomeric but in the presence of 1 equiv of Swa (K_L = 0.6 μM (*53*)) is 90% bound dimer (*23*).

Ser88Glu as a Phosphomimetic. Because of similarities of charge and side-chain length, glutamic acid is commonly used to mimic phosphoserine, and there is at least one example of a natural "phosphomimetic" mutation: in phosphorylase kinase, a glutamic acid residue in the activation loop replaces a conserved threonine that serves as a phosphorylation target in homologous kinases (*54*). $LC8_{S88E}$ has been used extensively in experiments both *in vitro* and *in vivo* to mimic phosphorylated wild-type LC8 (*26*). How appropriate is Glu88 as a model for LC8 phosphoserine-88? Glu88 is partially buried at the dimer interface and incurs only a small steric penalty. Phosphoserine is composed of heavier atoms and one additional atom and therefore may incur a larger steric penalty. Phosphoserine can have up to two negative charges, and the first acid dissociation constant ($pK_{a1} = 2$) ensures that, even if its pK_a is perturbed by several pH units in the dimer, phosphoserine always has at least one negative charge at neutral pH (*55*). Thus we conclude that the K_D of wild-type LC8 with one subunit phosphorylated is at least as high as that of $LC8_{S88E}$ with one Glu88 residue deprotonated (28 μM; Table 3) and possibly higher due to steric effects and/or greater charge. By the same argument, we expect the K_D of doubly phosphorylated LC8 at neutral pH to be at least as high as that of $LC8_{S88E}$ when both Glu88 residues are deprotonated (59 mM; Table 3), and we expect the dimerization transition state energy in phosphorylated LC8 to be at least as high as that in $LC8_{S88E}$, leading to similarly slower association kinetics compared to wild-type LC8.

Functional Implications. The LC8 dimer has two identical phosphorylation sites, one on each subunit. Does regulation require phosphorylation of both sites or is phosphorylation of just one sufficient? Phosphorylation of multiple sites is a way to achieve cooperativity in response to kinase activity and has been demonstrated in other systems such as the MAPK signaling protein Ste5 (*56*). On the basis of our studies with $LC8_{S88E}$, we conclude that for a heterodimer of phosphorylated and unphosphorylated LC8 K_D is 28 μM or higher (Table 3); therefore, phosphorylation of one subunit is sufficient to prevent formation of the apo-LC8 dimer at physiological concentration. Different behavior may occur in the presence of ligands. Swa and the apoptotic factor Bim both bind with affinities better than 1 μM (*53*) and, therefore, when present at 10 μM decrease the apparent dimer dissociation constant by a factor of 100 (eq 11). Tightly binding ligands such as these may overcome the energetic penalty to dimerization due to phosphorylation of one subunit and allow formation of singly phosphorylated heterodimers of LC8, whereas more weakly binding ligands such as the dynein intermediate chain (IC) may not. Thus the presence of two identical phosphorylation sites on LC8 provides this hub protein with a mechanism to regulate its diverse ligands differently in response to phosphorylation.

ACKNOWLEDGMENT

We acknowledge the support of the nucleic acid and protein core and the mass spectrometry core in the OSU Environmental Health Sciences Center. We thank Yujuan Song and Jean Yau for protein preparation, Jessica Morgan for assistance in collecting NMR data, and the HHMI Undergraduate Summer Research program at OSU for providing mentorship.

SUPPORTING INFORMATION AVAILABLE

K_D, k_{on}, and k_{off} measurements for wild-type LC8 and $LC8_{S88E}$ (shown in Figure 4). This material is available free of charge via the Internet at http://pubs.acs.org.

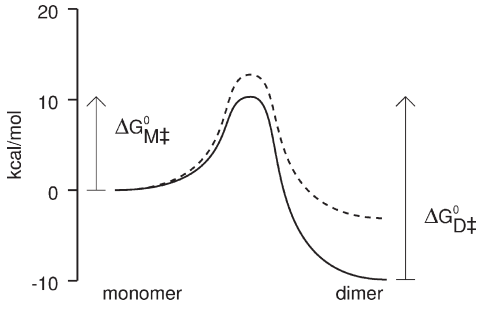

FIGURE 6: Energetic consequences of the Ser88Glu mutation at neutral pH. Free energies for monomer, dimer, and transition state were calculated from the model for wild-type LC8 (solid line) and for $LC8_{S88E}$ (dashed line).

Scheme 2: LC8 Dimerization Coupled to Ligand Binding[a]

$$2M \overset{K_D}{\rightleftharpoons} D \overset{K_L}{\rightleftharpoons} DL \overset{K_L}{\rightleftharpoons} DL_2$$

[a]Abbreviations: M, LC8 monomer; D, LC8 dimer; L, ligand; K_D, dimer dissociation constant; K_L, ligand-binding constant.

REFERENCES

1. Pfister, K., Fisher, E., Gibbons, I., Hays, T., Holzbaur, E., McIntosh, J., Porter, M., Schroer, T., Vaughan, K., Witman, G., King, S., and Vallee, R. (2005) Cytoplasmic dynein nomenclature. *J. Cell Biol. 171*, 411–413.
2. Dick, T., Ray, K., Salz, H., and Chia, W. (1996) Cytoplasmic dynein (ddlc1) mutations cause morphogenetic defects and apoptotic cell death in *Drosophila melanogaster*. *Mol. Cell. Biol. 16*, 1966–1977.
3. Vallee, R., Williams, J., Varma, D., and Barnhart, L. (2004) Dynein: An ancient motor protein involved in multiple modes of transport. *J. Neurobiol. 58*, 189–200.
4. Benashski, S., Harrison, A., Patel-King, R., and King, S. (1997) Dimerization of the highly conserved light chain shared by dynein and myosin V. *J. Biol. Chem. 272*, 20929–20935.
5. Espindola, F., Suter, D., Partata, L., Cao, T., Wolenski, J., Cheney, R., King, S., and Mooseker, M. (2001) The light chain composition of chicken brain myosin-Va: calmodulin, myosin-II essential light chains, and 8-kDa dynein light chain/PIN. *Cell Motil. Cytoskeleton 47*, 269–281.
6. Makokha, M., Hare, M., Li, M., Hays, T., and Barbar, E. (2002) Interactions of cytoplasmic dynein light chains Tctex-1 and LC8 with the intermediate chain IC74. *Biochemistry 41*, 4302–4311.
7. Lo, K., Naisbitt, S., Fan, J., Sheng, M., and Zhang, M. (2001) The 8-kDa dynein light chain binds to its targets via a conserved (K/R)XTQT motif. *J. Biol. Chem. 276*, 14059–14066.
8. Hódi, Z., Németh, A., Radnai, L., Hetényi, C., Schlett, K., Bodor, A., Perczel, A., and Nyitray, L. (2006) Alternatively spliced exon B of myosin Va is essential for binding the tail-associated light chain shared by dynein. *Biochemistry 45*, 12582–12595.
9. Wagner, W., Fodor, E., Ginsburg, A., and Hammer, J. (2006) The binding of DYNLL2 to myosin Va requires alternatively spliced exon B and stabilizes a portion of the myosin's coiled-coil domain. *Biochemistry 45*, 11564–11577.
10. Schnorrer, F., Bohmann, K., and Niesslein-Volhard, C. (2000) The molecular motor dynein is involved in targeting swallow and bicoid RNA to the anterior pole of *Drosophila* oocytes. *Nat. Cell Biol. 2*, 185–190.
11. Naisbitt, S., Valtschanoff, J., Allison, D., Sala, C., Kim, E., Craig, A., Weinberg, R., and Sheng, M. (2000) Interaction of the postsynaptic density-95/guanylate kinase domain-associated protein complex with a light chain of myosin-V and dynein. *J. Neurosci. 20*, 4524–4534.
12. Lo, K., Kan, H., Chan, L., Xu, W., Wang, K., Wu, Z., Sheng, M., and Zhang, M. (2005) The 8-kDa dynein light chain binds to p53-binding protein 1 and mediates DNA damage-induced p53 nuclear accumulation. *J. Biol. Chem. 280*, 8172–8179.
13. King, S., Barbarese, E., Dillman, J., Patel-King, R., Carson, J., and Pfister, K. (1996) Brain cytoplasmic and flagellar outer arm dyneins share a highly conserved Mr 8,000 light chain. *J. Biol. Chem. 271*, 19358–19366.

14. Jaffrey, S., and Snyder, S. (1996) PIN: An associated protein inhibitor of neuronal nitric oxide synthase. *Science 274*, 774–777.
15. Wang, L., Hare, M., Hays, T., and Barbar, E. (2004) Dynein light chain LC8 promotes assembly of the coiled-coil domain of swallow protein. *Biochemistry 43*, 4611–4620.
16. Barbar, E. (2008) Dynein light chain LC8 is a dimerization hub essential in diverse protein networks. *Biochemistry 47*, 503–508.
17. Barbar, E., Kleinman, B., Imhoff, D., Li, M., Hays, T., and Hare, M. (2001) Dimerization and folding of LC8, a highly conserved light chain of cytoplasmic dynein. *Biochemistry 40*, 1596–1605.
18. Nyarko, A., Cochrun, L., Norwood, S., Pursifull, N., Voth, A., and Barbar, E. (2005) Ionization of His 55 at the dimer interface of dynein light-chain LC8 is coupled to dimer dissociation. *Biochemistry 44*, 14248–14255.
19. Wang, W., Lo, K., Kan, H., Fan, J., and Zhang, M. (2003) Structure of the monomeric 8-kDa dynein light chain and mechanism of the domain-swapped dimer assembly. *J. Biol. Chem. 278*, 41491–41499.
20. Makokha, M., Huang, Y., Montelione, G., Edison, A., and Barbar, E. (2004) The solution structure of the pH-induced monomer of dynein light-chain LC8 from *Drosophila*. *Protein Sci. 13*, 727–734.
21. Benison, G., Karplus, P., and Barbar, E. (2007) Structure and dynamics of LC8 complexes with KXTQT-motif peptides: Swallow and dynein intermediate chain compete for a common site. *J. Mol. Biol. 71*, 457–468.
22. Benison, G., Karplus, P., and Barbar, E. (2008) The interplay of ligand binding and quaternary structure in the diverse interactions of dynein light chain LC8. *J. Mol. Biol. 384*, 954–966.
23. Song, Y., Benison, G., Nyarko, A., Hays, T., and Barbar, E. (2007) Potential role for phosphorylation in differential regulation of the assembly of dynein light chains. *J. Biol. Chem. 282*, 17272–17279.
24. Puthalakath, H., Huang, D., O'Reilly, L., King, S., and Strasser, A. (1999) The proapoptotic activity of the Bcl-2 family member Bim is regulated by interaction with the dynein motor complex. *Mol. Cell 3*, 287–296.
25. Vadlamudi, R., Bagheri-Yarmand, R., Yang, Z., Balasenthil, S., Nguyen, D., Sahin, A., den Hollander, P., and Kumar, R. (2004) Dynein light chain 1, a p21-activated kinase 1-interacting substrate, promotes cancerous phenotypes. *Cancer Cell 5*, 575–585.
26. Song, C., Wen, W., Rayala, S., Chen, M., Ma, J., Zhang, M., and Kumar, R. (2008) Serine 88 phosphorylation of the 8-kDa dynein light chain 1 is a molecular switch for its dimerization status and functions. *J. Biol. Chem. 283*, 4004–4013.
27. Lightcap, C., Sun, S., Lear, J., Rodeck, U., Polenova, T., and Williams, J. (2008) Biochemical and structural characterization of the Pak1-LC8 interaction. *J. Biol. Chem. 283*, 27314–27324.
28. Liang, J., Jaffrey, S., Guo, W., Snyder, S., and Clardy, J. (1999) Structure of the PIN/LC8 dimer with a bound peptide. *Nat. Struct. Biol. 6*, 735–740.
29. Lin, K., Rath, V., Dai, S., Fletterick, R., and Hwang, P. (1996) A protein phosphorylation switch at the conserved allosteric site in GP. *Science 273*, 1539–1542.
30. Becker, S., Groner, B., and Mller, C. (1998) Three-dimensional structure of the Stat3β homodimer bound to DNA. *Nature 394*, 145–151.
31. Antz, C., Bauer, T., Kalbacher, H., Frank, R., Covarrubias, M., Kalbitzer, H., Ruppersberg, J., Baukrowitz, T., and Fakler, B. (1999) Control of K^+ channel gating by protein phosphorylation: Structural switches of the inactivation gate. *Nat. Struct. Biol. 6*, 146–150.
32. Sprangers, R., Velyvis, A., and Kay, L. (2007) Solution NMR of supramolecular complexes: Providing new insights into function. *Nat. Methods 4*, 697–703.
33. Benison, G., and Barbar, E. (2009) NMR analysis of dynein light chain dimerization and interactions with diverse ligands. *Methods Enzymol. 455*, 237–258.
34. Farrow, N. A., Zhang, O. W., Forman-Kay, J. D., and Kay, L. E. (1994) A heteronuclear correlation experiment for simultaneous determination of ^{15}N longitudinal decay and chemical-exchange rates of systems in slow equilibrium. *J. Biomol. NMR 4*, 727–734.
35. Otwinowski, Z., and Minor, W. (1997) Processing of X-ray diffraction data collected in oscillation mode. *Methods Enzymol. 276*, 307–326.
36. Vagin, A., and Teplyakov, A. (1997) MOLREP: An automated program for molecular replacement. *J. Appl. Crystallogr. 30*, 1022–1025.
37. Murshudov, G., Vagin, A., and Dodson, E. (1997) Refinement of macromolecular structures by the maximum-likelihood method. *Acta Crystallogr., Sect. D: Biol. Crystallogr. 53*, 240–255.
38. Emsley, P., and Cowtan, K. (2004) Coot: Model-building tools for molecular graphics. *Acta Crystallogr., Sect. D: Biol. Crystallogr. 60*, 2126–2132.
39. Winn, M., Isupov, M., and Murshudov, G. (2001) Use of TLS parameters to model anisotropic displacements in macromole cular refinement. *Acta Crystallogr., Sect. D: Biol. Crystallogr. 57*, 122–133.
40. Edelsbrunner, H., Facello, M., Fu, P., and Liang, J. Measuring proteins and voids in proteins, Proceedings of the 28th Annual Hawaii International Conference on System Sciences, Vol. *5*, pp 256−264.
41. The pymol molecular graphics system (http://www.delanoscientific.com/).
42. Tollinger, M., Kay, L., and Forman-Kay, J. (2005) Measuring pK(a) values in protein folding transition state ensembles by NMR spectroscopy. *J. Am. Chem. Soc. 127*, 8904–8905.
43. Camacho, C., Weng, Z., Vajda, S., and DeLisi, C. (1999) Free energy landscapes of encounter complexes in protein-protein association. *Biophys. J. 76*, 1166–1178.
44. Zhou, H. (2001) Disparate ionic-strength dependencies of on and off rates in proteinprotein association. *Biopolymers 59*, 427–433.
45. Davis, I., Leaver-Fay, A., Chen, V., Block, J., Kapral, G., Wang, X., Murray, L., Arendall, W., Snoeyink, J., Richardson, J., and Richardson, D. (2007) MolProbity: All-atom contacts and structure validation for proteins and nucleic acids. *Nucleic Acids Res. 35*, W375–383.
46. Rogers, N., Moore, G., and Sternberg, M. (1985) Electrostatic interactions in globular proteins: calculation of the pH dependence of the redox potential of cytochrome *c*551. *J. Mol. Biol. 182*, 613–616.
47. Russell, A., Thomas, P., and Fersht, A. (1987) Electrostatic effects on modification of charged groups in the active site cleft of subtilisin by protein engineering. *J. Mol. Biol. 193*, 803–813.
48. Alden, R., Parson, W., Chu, Z., and Warshel, A. (1995) Calculations of electrostatic energies in photosynthetic reaction centers. *J. Am. Chem. Soc. 117*, 12284–12298.
49. Mohan, P., and Hosur, R. (2008) NMR characterization of structural and dynamics perturbations due to a single point mutation in *Drosophila* DLC8 dimer: Functional implications. *Biochemistry 47*, 6251–6259.
50. Miloushev, V., Bahna, F., Ciatto, C., Ahlsen, G., Honig, B., Shapiro, L., and Palmer, A. (2008) Dynamic properties of a type II cadherin adhesive domain: Implications for the mechanism of strand-swapping of classical cadherins. *Structure 16*, 1195–1205.
51. Montelione, G., and Wagner, G. (1989) 2D chemical-exchange NMR spectroscopy by proton-detected heteronuclear correlation. *J. Am. Chem. Soc. 111*, 3096–3098.
52. Gabdoulline, R., and Wade, R. (2002) Biomolecular diffusional association. *Curr. Opin. Struct. Biol. 12*, 204–213.
53. Hall, J., Hall, A., Pursifull, N., and Barbar, E. (2008) Differences in dynamic structure of LC8 monomer, dimer, and dimer-peptide complexes. *Biochemistry 47*, 11940–11952.
54. Owen, D., Noble, M., Garman, E., Papageorgiou, A., and Johnson, L. (1995) Two structures of the catalytic domain of phosphorylase kinase: An active protein kinase complexed with substrate analogue and product. *Structure 3*, 467–482.
55. Xie, Y., Jiang, Y., and Ben-Amotz, D. (2005) Detection of amino acid and peptide phosphate protonation using Raman spectroscopy. *Anal. Biochem. 343*, 223–230.
56. Strickfaden, S., Winters, M., Ben-Ari, G., Lamson, R., Tyers, M., and Pryciak, P. (2007) A mechanism for cell-cycle regulation of MAP kinase signaling in a yeast differentiation pathway. *Cell 128*, 519–531.